3D structure and evolution of EUV bright points observed by STEREO/SECCHI/EUVI

Ryun-Young Kwon[1,2], Jongchul Chae[3], Joseph M. Davila[2], Jie Zhang[4], Yong-Jae Moon[5], Watanachak Poomvises[1,2], & Shaela I. Jones[2,6]

Catholic University of America and NASA Goddard Space Flight Center, Solar Physics Laboratory, Code 671, Greenbelt, MD 20771, USA

ABSTRACT

We unveil the three-dimensional structure of quiet-Sun EUV bright points and its temporal evolution by applying the triangulation method to images taken by SECCHI/EUVI on board STEREO twin spacecraft. For this study we examine the heights and lengths, as components of three-dimensional structure of EUV bright points and their temporal evolutions. Among them we present three bright points which show three distinct patterns of evolution. We show that the three distinct types (decreasing, increasing, and steady in height and length) of EUV bright points are consistent with photospheric motions (converging, diverging, and shearing, respectively) of their underlying magnetic flux concentrations. They all have multi-temperature loop systems in which hot loops are overlying cooler loops with a strong correlation between height and length. Both flux emergence and cancellation occur during their lifetimes: flux emergence is dominant in the initial phase and flux cancellation becomes significant when the radiance flux of a bright point reaches its maximum. Our results suggest that magnetic flux emergences may play an important role in magnetic reconnection and EUV bright points are semi-circular and multi-thermal structures connecting the two opposite magnetic poles, formed by magnetic reconnection.

---

[1]Department of Physics, Catholic University of America, 620 Michigan Avenue, Washington, DC 20064, USA

[2]NASA Goddard Space Flight Center, Solar Physics Laboratory, Code 671, Greenbelt, MD 20771, USA

[3]Astronomy Program, Department of Physics and Astronomy, Seoul National University, Korea

[4]School of Physics, Astronomy and Computational Sciences, George Mason University, Fairfax, VA 22030, USA

[5]School of Space Research, Kyung Hee University, Yongin 446-701, Republic of Korea

[6]Department of Physics, University of Maryland, College Park, MD 20740, USA

Subject headings: Sun: corona — Sun: transition region — Sun: UV radiation

1. INTRODUCTION

EUV bright points (hereafter BPs) are an ubiquitous feature which is observed in active Sun, quiet Sun, and coronal hole regions, with a typical temperature below 2 MK (Gloub et al. 1974; Zhang et al. 2001). It has been suggested that BPs should be a potential source to heat up the solar corona since the high temperature corona (>1 MK) is observed not only in active regions, but also in the quiet Sun (von Rekwski et al. 2006, and reference therein). Accordingly, there have been many observational and theoretical efforts to understand the nature of EUV and X-ray BPs, as follows.

BPs have been typically observed with emerging or canceling magnetic flux concentrations (e.g., Webb et al. 1993, and references therein). This observational fact suggests that the underlying magnetic fluxes of BPs should tell us the detailed processes of their formation, decay, and energization. BPs were observed in ephemeral active regions (Harvey et al. 1973; Gloub et al. 1974; Martin & Harvey 1979) consisting of several small emerging magnetic bipoles having a flux of about 10^{19} to 10^{20} Mx. Webb et al. (1993) reported that most of BPs are associated with two opposite magnetic flux concentrations converging and canceling, which is thought to be a cause of magnetic reconnection and subsequent submergence of magnetic fluxes (Chae et al. 2002, 2004). Recently, Madjarska et al. (2003) showed that a BP first appeared when two opposite magnetic flux concentrations were about 7000 km apart and disappeared around the time when one flux concentration was fully canceled. In addition, they found that there is a remarkable correlation between the radiance flux of a BP and the unsigned total magnetic flux during its life.

Based on the observational facts described above, several theoretical models have explained the formation and evolution of BPs. Priest et al. (1994) proposed a model, the so-called converging flux model, in order to explain observational reports of the converging and canceling small magnetic flux concentrations. In contrast, the separator reconnection model propounded by Longcope (1998) suggests shearing motions of photospheric magnetic flux concentrations with background magnetic fields as a necessary condition for the occurrence of magnetic reconnection. These two models have been strongly constrained by the three-dimensional structure of BPs. For instance, the converging flux model predicts that the geometry of a subsequent BP is determined by the distance of an underlying magnetic bipole and its height should be reduced owing to converging magnetic flux (Kwon et al. 2010), while the separator reconnection model allows the size of a BP to exceed the distance of two magnetic flux concentrations so that there is no necessity to reduce its height (Longcope et

al. 2001), as the two magnetic flux concentrations converge.

Recently, the first stereoscopic analysis of BPs using simultaneous observation performed by STEREO/SECCHI/EUVI was done by Kwon et al. (2010). According to their results, the BPs seen in the 171 Å, 195 Å, and 284 Å images are loop-shaped and their average heights are 5.1, 6.7, and 6.1 Mm, respectively. The BPs in the 304 Å images are the lowest with an average of 4.4 Mm, among the four passbands and are commonly associated with the legs of the loop-shape BPs. The heights of the loops are approximately half of the lengths. These characteristics are similar to the semi-circular loops and temperature stratification found in the flaring loop reported by Masuda et al. (1994). Because of these consistency, it may be concluded that an BP is a flaring-like loop system having magnetic reconnection origin.

The main purpose of the present work is to reveal the evolution of three-dimensional structures of EUV BPs, in terms of the height and the length. In addition, the physical properties of the underlying magnetic flux concentrations are inspected to see what determines and changes their three-dimensional structures. Finally, we present three distinct changes in heights : decreasing, increasing, and steady. The next section describes the data and method to determine the three-dimensional structures of BPs and to measure the magnetic properties of the underlying magnetic flux concentrations. Section 3 shows three different types of evolutions in the height variations and Section 4 is devoted to detailed discussions on our findings. Finally, a brief conclusion is given in Section 5.

2. DATA AND ANALYSIS

The heights, lengths, and intensities of EUV BPs are measured using data sets taken by the Extreme UltraViolet Imager (EUVI; Wülser et al. 2004) on board the Solar TErrestrial RElations Observatory (STEREO) spacecraft (Howard et al. 2008). STEREO consists of twin spacecraft moving ahead (hereafter SC/A) and behind (SC/B) the Earth around the Sun. EUVI instruments provide two simultaneous solar images ($\pm 1.7\,R_{\odot}$) at different view points with four passbands, 171, 195, 284, and 304 Å. We used the data sets taken from 21 to 23 March 2008 and the separation angle of the two spacecraft was about 47°. Since the SC/A and B are located at different distance from the Sun, they have different spatial resolutions. The pixel size of EUVI instruments is 1.6″, the distances of the SC/A and B from the Sun were 1.44×10^8 km and 1.51×10^8 km at that time, and one pixel of SC/A and B correspond to about 1.11 Mm and 1.16 Mm, respectively. The time cadences of the images at 171, 195, 284, and 304 Å were typically 2.5, 10, 20, and 2.5 or 10 min, respectively. We used full-disk 1-minute magnetograms by SOHO/MDI in order to examine the properties of photospheric magnetic fluxes. Although the magnetogram has a relatively low pixel resolution (about 2 arc

second or 1.39 Mm), it has a high time cadence (about 1 minute) and we could expect that the time variations of magnetic flux concentrations can be well traced.

We employed a method developed by Kwon et al. (2010) to measure the heights of BPs. A sequence of sub-images centered on a BP is extracted with a size of 32 by 32 pixels and the background emission and noise are removed. After that the true signal of the BP is obtained and the center of the BP is determined by the center of gravity method. The two lines of sight connecting two spacecraft and the centers of a BP are determined and the height is measured by determining the skew of the two lines of sight. After subtracting the background and the noise from an original image, the length and integrated radiance flux of a BP are measured. The length of a BP is defined as the maximum length between two points comprising the boundary of a BP on SC/A and B images, since the projection effect may reduce the length on an image plane. The radiance flux is defined as the sum of intensities over the pixels inside the boundary of a BP on SC/A image. A detailed explanation of the method is given in Kwon et al. (2010).

Now, we would like to explain a method to determine the photospheric magnetic flux and distance between two opposite magnetic flux concentrations associated with a BP. In order to minimize the geometrical distortion of longitudinal magnetic fields depending on the position on the solar disk, we only selected BPs whose heliolongitudes are equal to or less than 30 degree. We took averages over three frames taken within three minutes to remove high frequency features near the underlying magnetic flux concentrations. Moreover, pixels with the unsigned values below 15 G are set to zero. The center of each magnetic element is determined by the center of gravity method and the distance represents the length between the two centers projected on the image plane. Finally, magnetic flux of each pole is determined by integrating the flux density over the region masked.

Meanwhile, we need to correct the recorded time on each spacecraft. Since the distances between the Sun and the spacecraft are generally different, the light traveling times are different and the times recorded in the fits headers may be different from one another for a specific event. In order to remove this discrepancy, each time is corrected by assuming that all spacecraft are located at the distance of the Earth.

3. Results

We measured the heights of 13 EUV BPs during their lifetimes. The lifetimes range from 9 to 47 hr with an average of 20 hr and the heights are in the range of 4 to 18 Mm with an average of 8 Mm. Our analysis reveals that there exist all possible height changes:

increasing (5 events), decreasing (4 events), and steady (4 events). It is interesting to note that there are no dominant patterns. In order to carry out a detailed study of the evolution of BPs, we selected three BPs from each type whose heliolongitudes on the MDI magnetograms are near the central meridian. In the following three sections, we show the evolution of three BPs focusing on the 195 Å passband. Case A, B and C refer to the three types of BPs, increasing, decreasing, and steady, respectively.

3.1. Case A

The first case shows the typical pattern predicted by converging flux model (Priest et al. 1994) in the temporal variation of its three dimensional structure. Figures 1 and 2 show that this BP is a faint and large loop system in the initial phase, for instance at (a), and evolve into a brighter and smaller one (b - e). The top panel in Figure 1 shows the height, half-length, and integraed radiance flux variations of this BP. The height and half-length are initially about 13 Mm and continuously decreases to about 6 Mm. The radiance flux is about 5×10^3 DN s^{-1} at (a) and significantly increases from (b). It has several peaks from near (a) to (e) and finially decrease from around (e). The first two columns in Figure 2 shows the BP observed by SC/B and A at the times (a) to (f) marked in Figure 1.

The two underlying magnetic flux concentrations are placed 17 Mm apart initially and converge each other to a distance of about 8 Mm. They are in a direction of the north - south at (a) and the axis of the loop system shows a consistency with the direction of the two opposite magnetic flux concentrations (Figure 1). The magnetic flux concentrations converge toward each other during the lifetime of 25 hr and the height and the size of the loop system decrease with distance simultaneously. Together with the converging motions, the magnetic flux concentrations also have weak shearing motions; the negative flux moves to the left-hand side of the positive patch and the axis of the loop system is rotated at the same time.

The magnetic flux concentrations are initially small and weak, and the positive flux is larger than the negative one at (a). After that, both fluxes grow up continuously from the time at (a) to (b) and new positive fluxes emerge at the left-hand side of the field of view at (b) in Figure 2. As a result, the loop system becomes a complicated one being made up of several loops, at least three. The negative flux decreases significantly from the time (d) and finally it almost disappeared.

The two opposite magnetic fluxes are initially unbalanced with the positive flux larger than the negative flux. The positive flux increases until t=10 hr and changed little for the

rest of its lifetime while the negative flux starts to decrease from that time.

3.2. Case B

The lifetime of case B is 47 hr which is about twice of case A. This BP comes into sight first as a small and faint loop system with a height of 10 Mm and turns out to be a large and bright loop system with a height of 14 Mm, which is different from case A. Figures 3 and 4 show complicated changes in its height.

The positive and negative magnetic flux concentrations seen in Figure 4 are aligned in the direction at 5 o'clock, as is the axis of the BP. The separation distance of the bipole increases from (a) to (d) and the size of the BP increases at the same time. On the other hand, the later phase of the evolution, from (d) to (f), shows that the separation distance and the size of the BP decrease together.

Case B in common with case A, shows the magnetic flux increase in the initial phase with the growth of the radiance flux. From (b) to (d), a new negative flux emerges at the upper right side of the image and a new loop system rises up between an old positive flux and the new negative flux at (c) and (d). The newly connected loop system is seen until the time (d), then it disappeared with its underlying negative flux.

3.3. Case C

Case C is clearly distinguished from cases A and B. As seen from Figure 5, its height changes little during its lifetime. The minimum height is about 8 Mm and the maximum height is about 10 Mm, so the variation in heights does not exceed 2 Mm. The change in half length is small with the minimum and maximum lengths of about 8 Mm and 12 Mm, respectively. The radiance flux variation is similar to those of the other cases; the BP first appeared as a faint loop system, reached its maximum radiance flux at (d) and then faded during the rest of its lifetime. Its lifetime is about 13 hr, the shortest among the three cases.

Small changes in the distance of the two opposite magnetic flux concentrations are found in consistency with the height and the length. In the initial phase, the separation distance in Figure 5 remains almost the same, but it begins to decrease a little at (c). After $t = 9$ hr, it seems to increase slightly.

Figure 6 suggests that this BP should be associated with a shearing motion of the photospheric magnetic fields. Initially, the negative and positive fluxes are aligned in the

north - south direction and then the negative flux moves to the right side of the positive flux. This motion is consistent with the orientation of the BP observed by SC/A and SC/B. The axis of the loop system is initially aligned in the direction at 7 o'clock and then, with the movements of the magnetic flux concentrations, the axis rotates counterclockwise. Its final orientation is at 4 o'clock.

The variation of the flux and the loop system are simpler than those of the other cases. Like the other cases, the flux increases in the initial phase and then decreases in its later half phase.

4. Discussion

In the previous section, we have presented the temporal evolution of the heights of three EUV BPs. Kwon et al. (2010) presented two ways to estimate the errors in heights. First one is an analytical way to derive an intrinsic error in carrying out a triangulation. This error depends on the separation angle (Θ) of the two spacecraft, the measurement error (Δ_2) in measuring a position on SC/B image, and the heliocentric angle (α_1) of an BP observed by SC/A. The distance error in the line of sight of SC/A is given by $\Delta X_1 = \Delta_2 / \sin\Theta$ and the height error Δh is approximately $\Delta X_1 \cos\alpha_1$. The separation angle of the two spacecraft during the observing period is about 47° and the measurement error Δ_2 is about 0.6 Mm (0.5 pixel on SC/B image), giving the intrinsic height error of about 0.82 Mm. Another one is an empirical way to estimate the measurement error in height using independent measurements at 195 Å and 284 Å bassbands and strong correlations between the two measurements. The two passpand images may represent plasma structures at similar temperatures so that the two heights may be well correlated with each other. The differences between the heights may be due to the intrinsic differences plus the random errors, so that the differences of the two heights can tell us the maximum random error. In this way, the measurement error is found to be about 0.86 Mm. From these two error analysis, we can conclude that the error in heights may not exceed 1 Mm.

One of the most prominent findings is that there are three distinct changes (decreasing, increasing, and steady) in height and length. Moreover, their changes are associated with the photospheric motions (converging, diverging, and shearing, respectively) of underlying magnetic flux concentrations. This consistency indicates that the three-dimensional structures are determined by the geometry of photospheric magnetic flux concentrations. Figure 7 shows three scatter plots of height vs. half-distance of magnetic flux separations for the three cases and positive correlations with the coefficients of 0.85, 0.52, and 0.48. The more direct comparison between the three-dimensional structures and the photospheric motions

is shown in Figure 8. As mentioned in the previous sections, the changes in length are consistent with the separation distance variations. More interestingly, it seems that the lengths of the BPs are within the range of the distances, suggesting that the BPs should be a loop system connecting the two opposite magnetic poles (cf. Longcope et al. 2001).

Second, there exist a couple of characteristics common to the three BPs, regardless of their distinct evolutions. (i) Each BP first appears as a faint loop system, its radiance flux reaches the maximum at the middle of its lifetime, and then it disappears as a faint loop system. (ii) The flux emergence is typically dominant in the initial phase and the flux decreases in the later phase. As a result, the radiance flux has a maximum near when the flux changes from increasing to decreasing and the radiance flux and the magnetic flux may be well correlated (Madjarska et al. 2003). These observational facts suggest that magnetic flux emergences play an important role in triggering magnetic reconnection which heats up plasmas in the initial phases and the rate of flux submergences (Chae et al. 2002, 2004) becoming higher than the one of flux emergences due to magnetic reconnection may appear as flux cancellations in the later phases.

Finally, we found no correlations between the variations of magnetic fluxes and three dimensional structures. In case A, the height and length significantly decrease in the initial phase but the total magnetic flux increases simultaneously while the height/length and the total magnetic flux increase together in the initial phase of case B. Furthermore, the total magnetic flux of case C significantly increases in the first half and then decreases in the second half, but there is no significant change in the three dimensional structure during its lifetime. In a similar way, there exists no correlation between the three dimensional structure and the radiance flux. This finding indicates that the three dimensional structure of BPs is mainly determined by the geometry of the two opposite magnetic flux concentrations rather than the amount of magnetic fluxes.

Our findings suggest that magnetic reconnection should be due to all kinds of photospheric motions including converging motions. Priest et al. (1994) proposed a converging flux model in which magnetic flux concentrations of opposite polarities initially unconnected approach each other and magnetic reconnection can occur at an X-type null point. As a consequence of magnetic reconnection, the two opposite magnetic flux concentrations are connected by magnetic field lines below the X-type null point, and the plasmas near the reconnected magnetic field lines are heated to have X-ray and/or EUV emissions. According to this scenario, the maximum height of the emission should be equal to half of the separation distance of two moving magnetic flux concentrations so that the height of a BP may decrease during its lifetime owing to converging motions, as seen in case A (Figure 1). However, case B shows diverging motions associated with the increasing lengths of BPs, indicating that the

converging motion may not be a necessary and sufficient condition for magnetic reconnection. Nevertheless, we cannot discard the converging motions as a driving source of magnetic reconnection process, taking into account the size of two opposite magnetic fluxes. In case one or both magnetic flux concentrations emerge through the photosphere with diverging motions, the fluxes and sizes of the concentrations may increase and it may be an alternative effect of converging magnetic fluxes. For instance, there are no significant increases in the minimum distances of cases B in the initial (diverging) phase as shown in Fgiure 8, implying that the two poles are diverging with flux emergences.

A separator reconnection model can explain the magnetic reconnection under the shearing motions including the converging and diverging motions (Longcope 1998). Magnetic reconnection occurs on the separator field lines owing to the interaction between initially unconnected two opposite magnetic flux concentrations and horizontal background magnetic fields and could heat up the plasmas along this separator. As a result, the three dimensional structure of subsequent X-ray/EUV BPs depends on the geometry of the separator. Since this geometry is different from the one of magnetic field lines connecting a bipole, the length of BPs could be longer than the separation distance. Longcope et al. (2001) showed that a portion of 37% of BPs which were investigated are longer than the bipole separations. However, our results seen in Figure 8 show that the lengths of BPs do not exceed the separation distances, which indicates that the BPs are the proxy of the magnetic field lines. Nevertheless, we cannot rule out this model because the difference of geometries between the magnetic field lines and the separator field lines may be small in general (Longcope 1998). It may be hard to resolve the geometrical differences between them in our measurements. As a matter of fact, the converging flux model and the separator reconnection model do not consider the internal structure of magnetic poles. Thus we think that it is necessary to look into more investigations taking the size of magnetic poles into account, considering magnetic flux emergences and cancellations.

Our findings suggest that magnetic flux emergences and cancellations of photospheric magnetic flux concentrations are crucial to understanding magnetic reconnection to form X-ray/EUV BPs and the geometry of the flux concentrations determines the three dimensional structure of BPs. From previous discussions, one may wonder if the characteristics of BPs are only determined by the properties of the underlying magnetic flux concentrations without background magnetic fields. As a matter of fact, the role of background magnetic fields in magnetic reconnection can be checked in terms of interaction distances which indicate the maximum distance between initially unconnected opposite magnetic flux concentrations to reconnect each other in the solar corona (Priest et al. 1994; Longcope 1998; Longcope et al. 2001). BPs may be the proxy of reconnected magnetic field lines and the length of BPs should be less than or equal to the interaction distance, so that the length may represent

the interaction distance. According to magnetic reconnection models (Priest et al. 1994; Longcope 1998), the interaction distance, D is given by the photospheric magnetic flux, Φ and the background magnetic field strength, B_0, that is, $D \sim \sqrt{\Phi/B_0}$. Taking a maximum flux $\Phi_> \equiv \max(\Phi_+, \Phi_-)$ as a photospheric magnetic flux Φ and a length as interaction distances (Longcope et al. 2001), we determined background magnetic fields. Figure 9 shows the determined background magnetic field, for the three BPs, as a function of height. The averages of the background magnetic fields are 14.1, 4.1, and 9.0 G, corresponding to the average heights of 8.49, 8.96, and 8.66 Mm, respectively. Interestingly, the background field strengths in this figure show decreasing patterns with heights as we expected in potential field extrapolations as well as in real solar corona. The correlation coefficients between B_0 and $1/h^2$ are 0.70, 0.55, and 0.22, respectively. Note that the heights, lengths, and magnetic fluxes are independently measured. This consistency may demonstrate that the interaction between the background magnetic fields and the photospheric magnetic fluxes is a crucial role in magnetic reconnection processes.

In addition, we also investigated the multi-thermal nature of EUV BPs using four passband images and our results are consistent with the previous study done by Kwon et al. (2010) which investigated 210 EUV BPs. They found that the lengths are about twice the heights and the height and morphology depend on passbands (temperature), indicating that an BP is a semi-circular and multi-temperature loop system. Note that they selected different BPs from 11 snapshot images separated by about a month, regardless of their evolutionary phases. Hence, it may be difficult to conclude that their findings are general characteristics over whole lifetimes of BPs. Figure 10 shows the height differences among three passbands during lifetimes. The heights of BPs at 195 Å are systematically higher than those at 171 Å and the BPs at 304 Å are located at the lowest part of these structures. These differences can be interpreted as overlying (195 Å), underlying (171 Å), and leg (304 Å) structures of a loop system (Kwon et al. 2010). Figure 11 shows scatter plots of height and half-lengths and the correlation coefficients are 0.79, 0.47, and 0.20, respectively. The correlation coefficient for case A is highest because this BP shows a single loop system during its lifetime except time (b) and (c) in Figure 2. The reason why case C has the lowest coefficient may be the smallest standard deviation (0.5 Mm) of heights since case C shows no significant changes in its height. Even with the small correlation coefficient of case C, this figure demonstrates that the heights and half-lengths are nearly identical in all cases. Our results demonstrate that the multi-temperature and semi-circular loop system is more or less a general character of BPs.

5. Summary and Conclusion

We have presented three-dimensional structure and evolution of EUV BPs, observed by STEREO/SECCHI/EUVI. We investigated the heights and the lengths as the components of the three-dimensional structures of BPs and found out the presence of three distinct changes in the heights and the lengths (decreasing, increasing, and steady). These types are associated with the converging, diverging, and shearing motions of underlying magnetic flux concentrations, respectively. It is significant that the height and the length are well correlated with the separation distance of two opposite magnetic flux concentrations and all the lengths of BPs seem to be less than or equal to the separation distances. These facts demonstrate that the three dimensional structures are determined by the geometry of underlying magnetic flux concentrations and BPs are a loop system connecting the two opposite magnetic poles. Irrespective of the distinct types, common evolutionary features are found in the radiance fluxes of BPs and the magnetic fluxes of underlying magnetic flux concentrations. In addition, they all have multi-temperature structures whose hot loops are overlying cooler loops with a remarkable correlation with the heights and the lengths. We could not find out direct relationships between the three-dimensional structure and the amount of magnetic fluxes. We compared the characteristics of the three BPs with two models, the converging flux model and the separator reconnection model, and we found that some our findings are consistent with these models. However, the emergence and the internal structure of underlying magnetic flux concentrations which are neglected in these models seem to be significant for the formation and the evolution of BPs. As a conclusion, BPs may be regarded as multi-thermal and semi-circular loop systems, like flaring loops, connecting two underlying magnetic concentrations, formed by magnetic reconnection due to the interaction between emerging magnetic fluxes and background magnetic fields.

This work was supported by NASA grant NNX10AN10G and the Korea Research Foundation Grant funded by the Korean Government (KRF-2008-220-C00022) .

REFERENCES

Chae, J., Moon, Y.-J., Wang, H., & Yun, H. S. 2002, Sol. Phys. 207, 73

Chae, J., Moon, Y.-J., & Pevtsov, A. A 2004, ApJ 602, L65

Gloub, L., Krieger, A. S., Silk, J. K., Timothy, A. F., & Vaiana, G. S. 1974, ApJ, 189, L93

Harvey, Karen L., & Martin, Sara F. 1973, Sol. Phys., 32, 389

Howard, R.A., et al. 2008, Space Sci. Rev. 136, 67

Kwon, R.-Y., Chae, J., & Zhang, J. 2010 ApJ, 714, 130

Longcope, D. W. 1998, ApJ, 507, 433

Longcope, D. W., Kankelborg, C. C., Lelson, J. L., & Pevtsov, A. A. 2001, ApJ, 553, 429

Madjarska, M. S., Doyle, J. G., Teriaca, L., & Banerjee, D. 2003, A&A, 398, 775

Martin, S. F., & Harvey, K. H. 1979, Sol. Phys., 64, 93

Masuda, S., Kosugi, T., Hara, H., Tsuneta, S., & Ogawara, Y. 1994, Nature, 371, 495

Priest, E. R., Parnell, C. E., & Martin, S. F. 1994, ApJ, 427, 459

von Rekowski, B., Parnell, C. E., & Priest, E. R. 2006, MNRAS, 366, 125

Webb, D. F., Martin, S. F., Moses, D., & Harvey, J. W. 1993 Sol Phys., 144, 15

Wülser, J.-P. eq al, 2004, SPIE, 5171, 111

Zhang, J., Kundu, M. R., & White, S. M. 2001, Sol. Phys., 198, 347

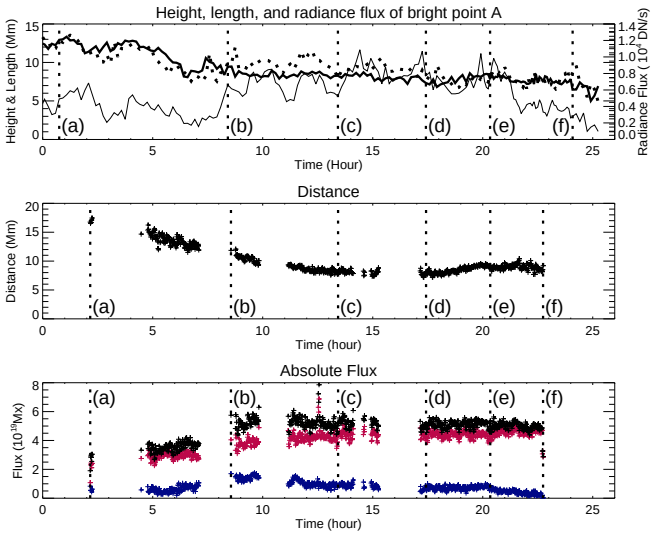

Fig. 1.— Temporal evolution of the physical parameters of the case A BP. The x-axis refers to the relative time from when the BP first appeared. The top panel shows the height (solid), half-length (dotted), and integrated radiance flux (thin-solid) variations. The middle panel represents the distance between two opposite magnetic flux concentrations in the unit of Mm and the bottom panel shows the unsigned magnetic flux variation in unit of 1×10^{19} Mx. The black, blue, and red colors refer to the magnetic flux, unsigned total, positive, and negative flux, respectively. The letters from (a) to (f) refer to the specific times which show some noticeable morphological changes (see text) in Figure 2.

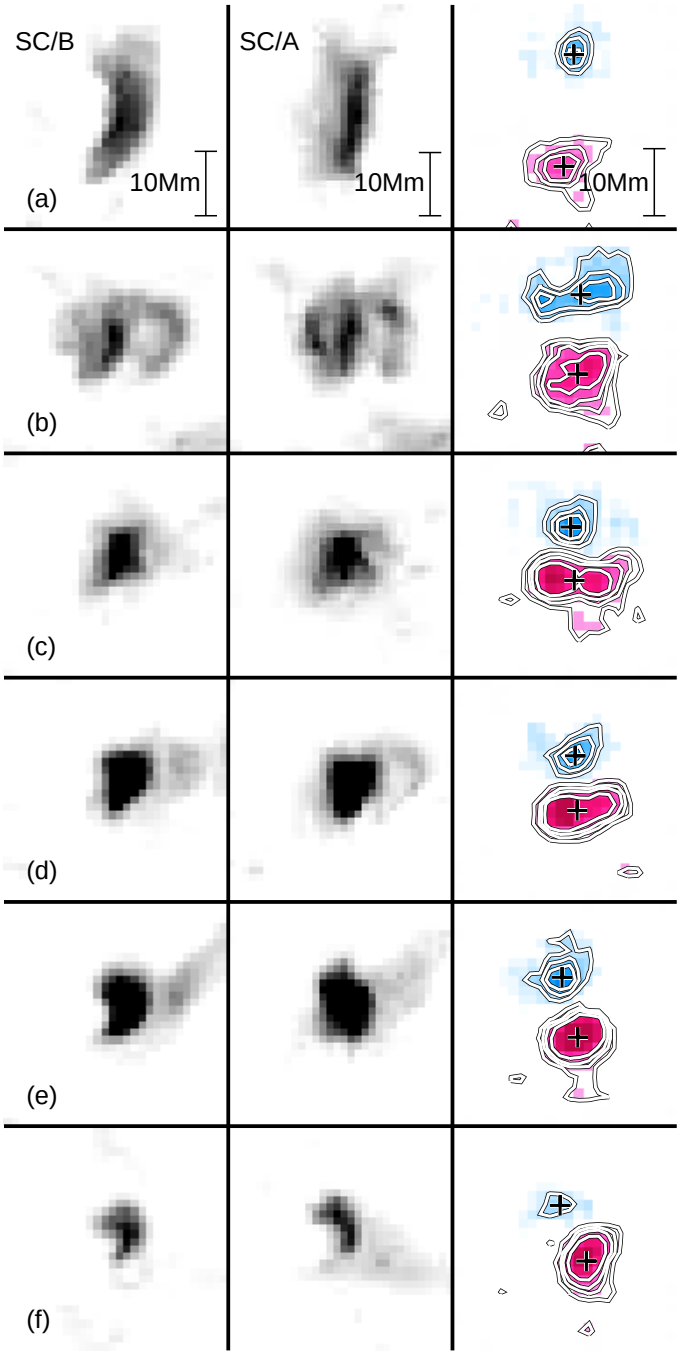

Fig. 2.— Morphological variation of the case A BP at the times (a) to (f) in Figure 1. The first and the second column show the BP observed by SC/A and SC/B, respectively. The third column shows a time series of photospheric longitudinal magnetograms observed by SOHO/MDI. Red and blue colors refer to the positive and negative fluxes.

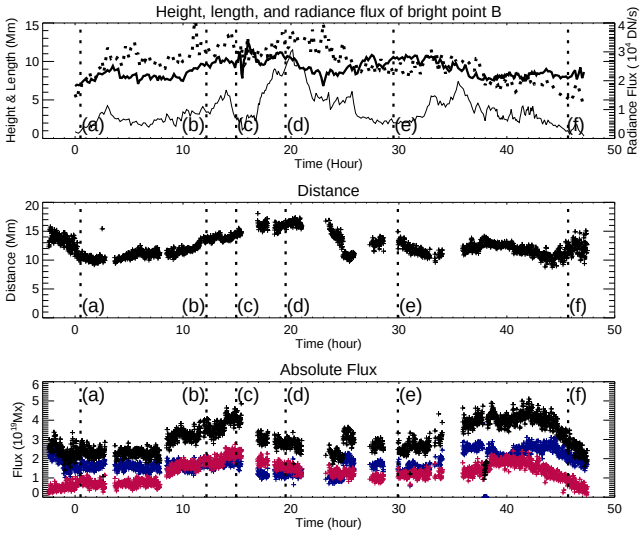

Fig. 3.— Temporal evolution of the physical parameters of case B. Other explanations are the same as Figure 1.

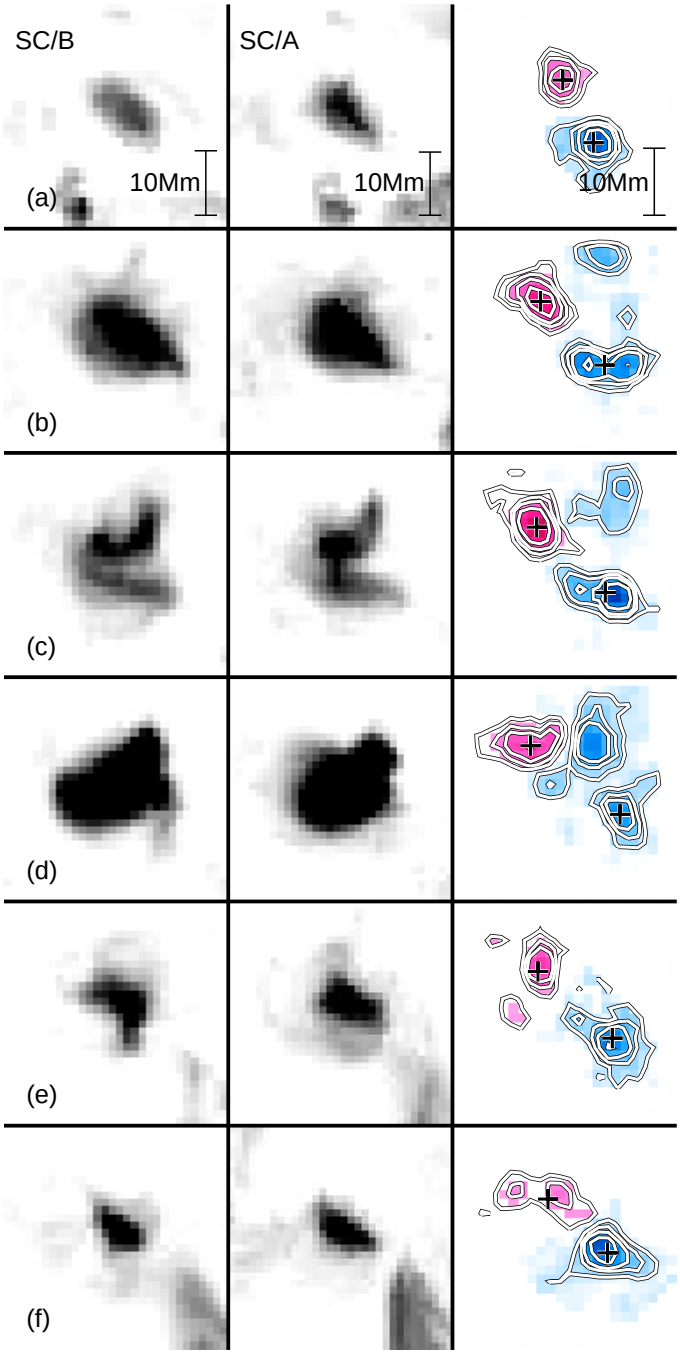

Fig. 4.— Morphological variation of case B at the time (a) to (f) in Figure 3. Other explanations are the same as Figure 2.

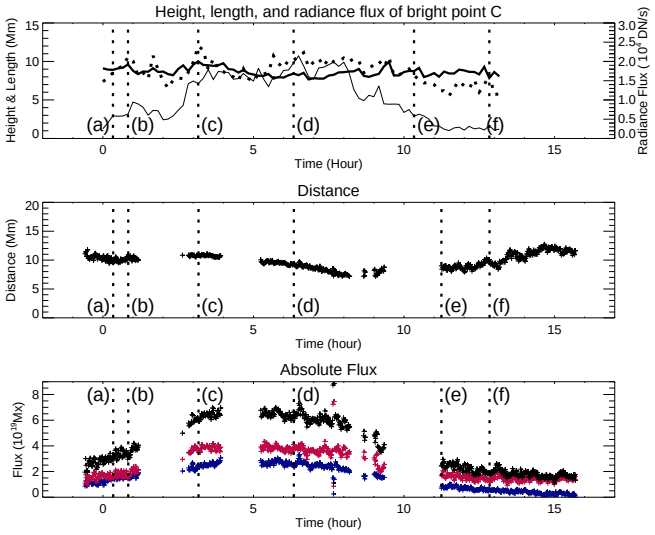

Fig. 5.— Temporal evolution of the physical parameters of case C. Other explanations are the same as Figure 1.

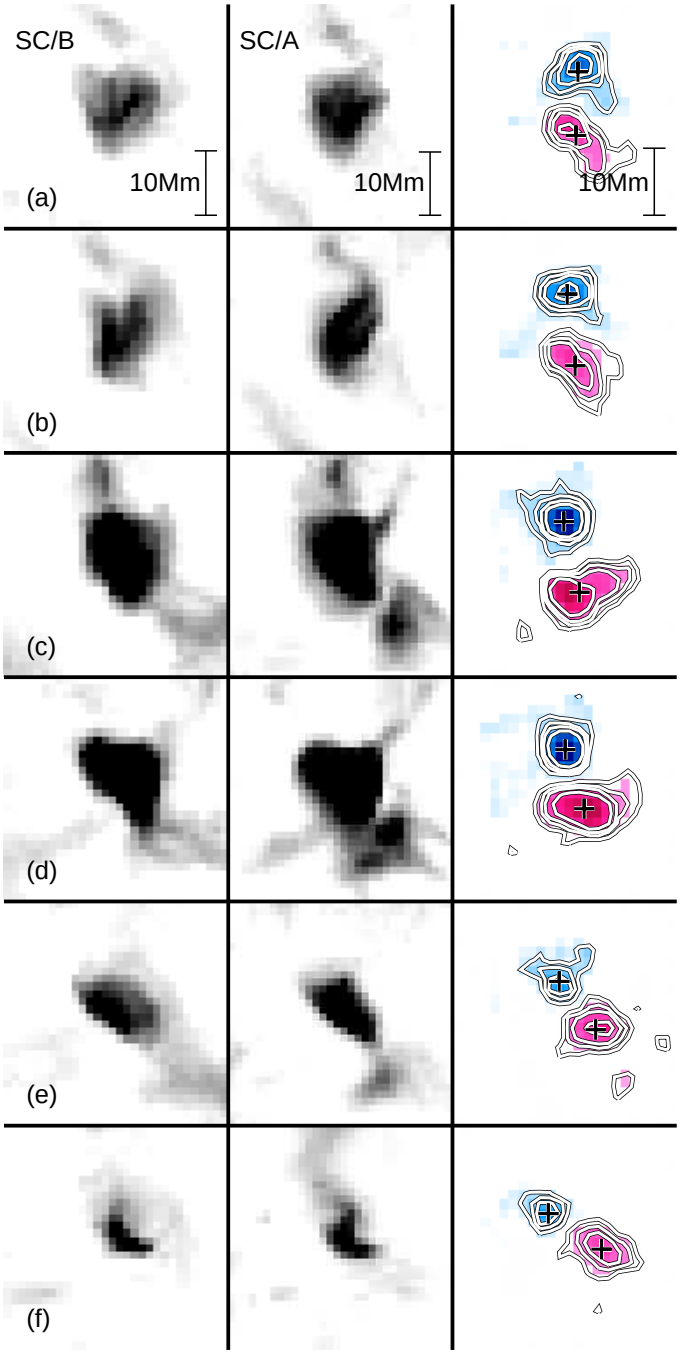

Fig. 6.— Morphological variation of case C at the time (a) to (f) in figure 5. Other explanations are the same as Figure 2.

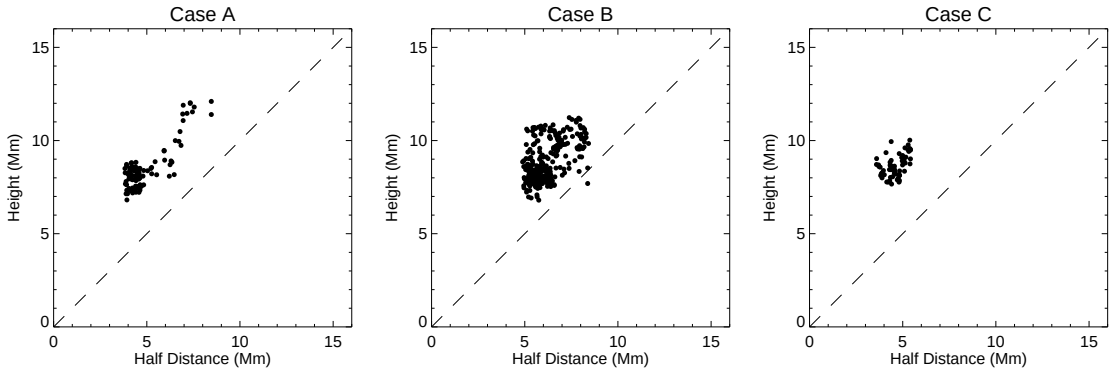

Fig. 7.— Scatter plots of height vs. half distance of underlying magnetic flux concentrations. The distances are measured from the center of a signed magnetic pole to the center of the opposite pole.

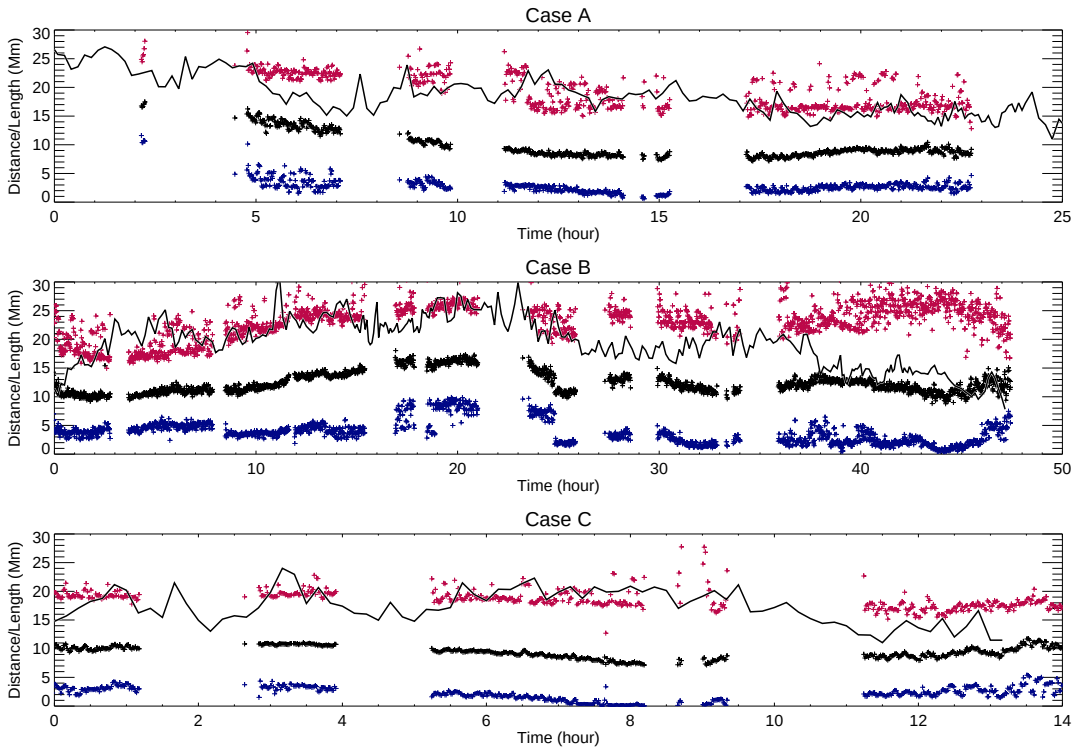

Fig. 8.— Time variations of lengths of BPs and distance of two opposite magnetic flux concentrations. The red, blue, and black crosses refer to the maximum, minimum, and center distances considering the sizes of the corresponding magnetic flux concentrations, respectively. The solid curves correspond to the lengths of the BPs.

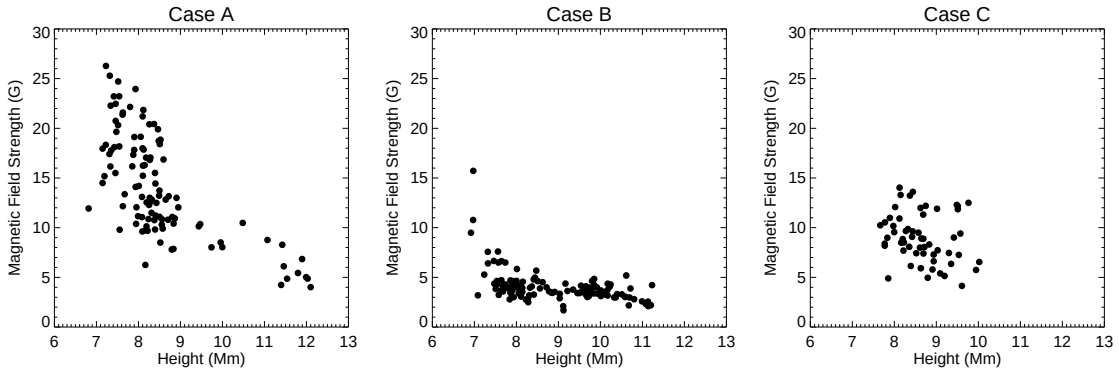

Fig. 9.— Scatter plots of background magnetic field strength vs. height for cases A to C, respectively.

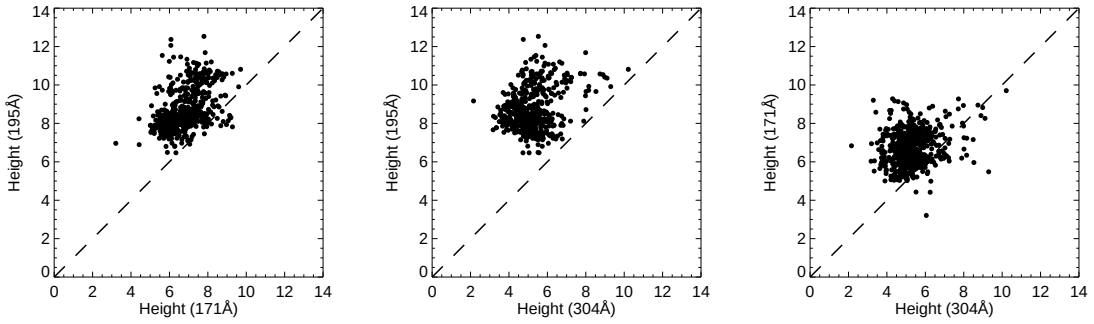

Fig. 10.— Scatter plots of heights at 195 Å vs. 171 Å (left), 195 Å vs. 304 Å (middle), and 171 Å vs. 304 Å (right) for all cases in each panel.

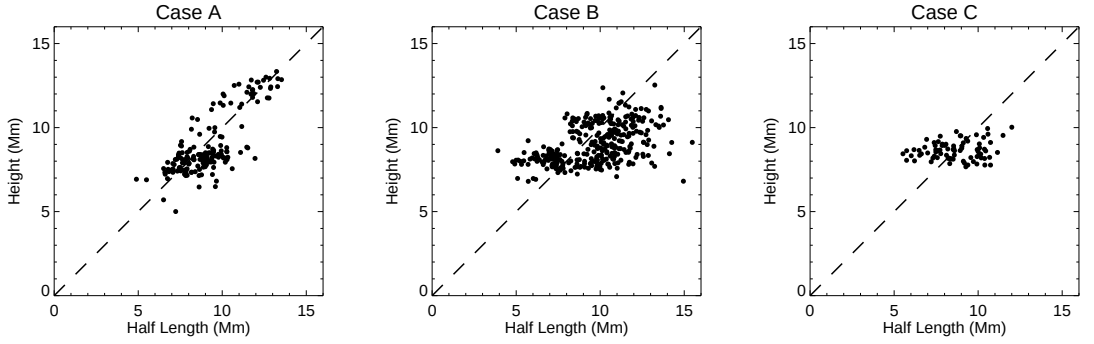

Fig. 11.— Scatter plots of height vs. half length for cases A to C, respectively.